Influence of oxygen partial pressure on the adsorption and diffusion during oxide growth: ZnO(0001) surface

Qiyuan Ruan, Jingchen Ye, Da-Jun Shu,* and Mu Wang†

National Laboratory of Solid State Microstructures and School of Physics, Nanjing University, Nanjing 210093, China and Collaborative Innovation Center of Advanced Microstructures, Nanjing University, Nanjing 210093, China

(Received 13 June 2016; revised manuscript received 17 February 2017; published 7 September 2017)

Oxygen partial pressure during vapor phase growth plays a critical role in determining the microstructure and other properties of oxides. However, it remains unclear how it affects the growth mechanism on the atomic scale. In this article, we take ZnO(0001) surface as a model case and demonstrate the influence of oxygen partial pressure on surface adsorption and diffusion of intrinsic adatoms by first-principles calculations. Two typical reconstructions of ZnO(0001) surface, denoted as (2×2)-O and n_3, are utilized to model the oxygen-rich condition and oxygen-poor condition, respectively. The (2×2)-O refers to the surface with an oxygen adatom in a (2×2) supercell, while the n_3 stands for the surface with triangular pits of edge length $n = 3$. We find that under the oxygen-rich condition in which (2×2)-O forms, adsorption of the O adatom is always more energetically favorable than the Zn adatom. Under oxygen-poor condition in which n_3 forms, however, the preferential adsorbate changes from O adatom to Zn adatom as the oxygen partial pressure decreases. The O adatom is less diffusive than the Zn adatom on both reconstructed surfaces. The diffusion barriers of both Zn and O on n_3 are higher than their counterparts on (2×2)-O. Insufficient surface diffusion leads to a high nucleation rate; therefore, a second-layer nucleus may form before the completion of the first-layer on n_3. It suggests that ZnO growth under oxygen-poor condition, in comparison with the oxygen-rich condition, is more likely to proceed with the three-dimensional island growth mode and result in a rougher surface.

DOI: 10.1103/PhysRevB.96.115412

I. INTRODUCTION

Metal oxides have attracted intensive attention due to their wide applications in optoelectronics, lasers, piezoelectronics, solar cells, and so on [1–7]. It is well known that properties of metal oxides are significantly influenced by the oxygen partial pressure during the vapor phase growth [8–18]. In complex oxides, for example, not only the interface conductivity, but also the sheet resistivity, Hall resistivity, and electron mobility of the thin film depend on the oxygen partial pressure [19]. It indicates that oxygen partial pressure affects the growth process and the interface structure [20–25]. To our best knowledge, however, few studies have been devoted to explore the influence of oxygen partial pressure on the atomistic process and the growth mechanism at the surface of metal oxide.

In this paper, we use zinc oxide (ZnO) as a model system to explore the influence of oxygen partial pressure during oxide growth. Fabrication of ZnO nanostructures has been widely reported motivated by their attractive applications. We have conducted the vapor growth of zinc oxide nanorods under different oxygen partial pressure. The larger density of the nucleus under smaller oxygen flux suggests that the surface kinetics is suppressed by decreasing oxygen partial pressure [26]. However, the corresponding microscopic growth mechanism has seldom been investigated [27–34]. Even the basic aspects of growth such as the adsorption and diffusion of adatoms remain unclear, partly because of the complexity of metal oxide surfaces and the difficulty of atomic-scale experiments [35,36].

Wurtzite-type zinc oxide prefers to grow in c axis with Zn-terminated (0001) and O-terminated $(000\bar{1})$ polar surfaces [27,31,32]. The alternately stacked Zn and O ionic layers along the c axis result in a net dipole field, which makes the polar surfaces unstable in the bulk-terminated form [35]. The proposed stabilization mechanisms include charge transfer from $(000\bar{1})$ to (0001) surface, formation of vicinal surfaces, and modifying the surface stoichiometry by surface reconstructions [37–43]. In the past decades, both theoretical calculations and experimental observations reported that oxygen adsorbed (2×2) reconstruction or triangular shaped holes can form on the ZnO(0001) surface, depending on the partial pressure of oxygen [40,42–45]. The different surface reconstructions under different oxygen partial pressure are expected to influence the surface kinetics and hence the growth mechanism.

In bulk ZnO, self-diffusion measurements of Zn and O have been widely reported with discrepancies in activation energy, which has been attributed to the different chemical potential of oxygen and Fermi level in different experiments by Erhart and Albe [46]. Experimentally, Azarov *et al.* recently confirmed that the diffusivity of Zn in bulk ZnO under O-rich condition is larger than under Zn-rich condition, because the diffusion of Zn is mediated by the Zn vacancy which is easier to form under O-rich condition [47]. For surface diffusion, so far we only find theoretical calculations. Huang *et al.* predicted that within the plane of the O-terminated ZnO(0001) surface, both oxygen vacancy and oxygen adatom are more diffusive than their zinc counterpart [48]. On the Zn-terminated ZnO(0001) surface, Fujiwara *et al.* proposed that Zn adatom is more diffusive than O according to their formation energies at several special adsorption sites of the ideal surface [49]. However, the influence of the oxygen partial pressure on the surface reconstruction and the intrinsic surface diffusion on ZnO(0001) surface remains uninvestigated.

*djshu@nju.edu.cn
†muwang@nju.edu.cn

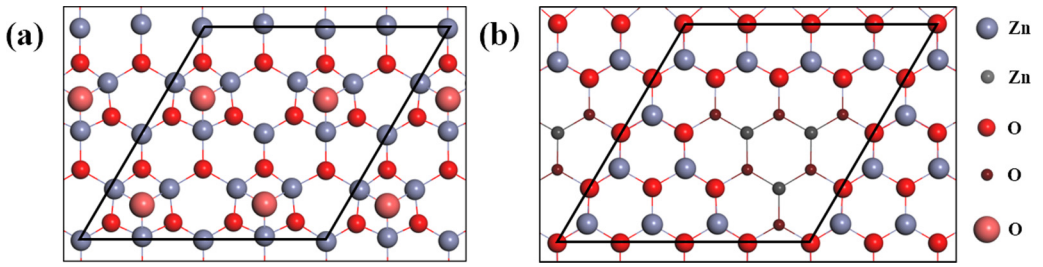

FIG. 1. Structures of the topmost layer of the two reconstructed ZnO(0001) surfaces: (a) oxygen-rich condition: (2 × 2)-O; (b) oxygen-poor condition: n_3. The z coordinates of surface atoms are schematically shown by the different sizes of the balls. Parallelogram boxes represent the (4 × 4) supercells used to model the surface adsorption and diffusion properties. Note that a (4 × 4) supercell consists of four unit cells of the (2 × 2)-O reconstruction, but only one unit cell of the n_3 reconstruction. Grey and red spheres are Zn and O atoms, respectively. Larger spheres means closer to the surface.

Based on density functional theory (DFT), in this article we study the adsorption and diffusion properties of zinc and oxygen atoms on the Zn-terminated ZnO(0001) surface under different oxygen partial pressure. Two typical reconstructions are taken as the substrate to cover the influence of partial oxygen pressure on the surface kinetics of ZnO. One is the surface with an oxygen adatom in each (2 × 2) supercell, denoted as (2 × 2)-O. The other is the reconstruction with an one-layer-deep triangular pit of edge length $n = 3$ in each (4 × 4) supercell, denoted as n_3. We find that adsorption of O atom is more favorable than Zn atom when (2 × 2)-O reconstruction is preferred. When n_3 reconstruction is preferred, however, the relative stability of Zn and O adatom depends on the oxygen partial pressure. As for the surface diffusion, O adatom is less diffusive than Zn adatom on both reconstructed surfaces. Moreover, the diffusion barriers of both Zn and O on n_3 are higher than the barriers on (2 × 2)-O. Since insufficient surface diffusion leads to a high nucleation rate, a second-layer nucleus may form before the first layer has been completed on n_3 surface [50,51]. It indicates that most probably the surface growth proceeds in the three-dimensional growth mode under the oxygen-poor condition, which results into a rougher surface morphology than that under oxygen-rich condition. We expect that the results are enlightening in understanding the microscopic growth mechanism of ZnO and other metal oxides under different oxygen atmosphere.

II. METHODS

The calculations are based on DFT implemented in the Vienna *ab initio* simulation package [52,53]. A plane wave basis set with cutoff energy of 550 eV is employed to expand the wave functions with the projector augmented wave method. We use the generalized gradient approximation according to Perdew-Wang-91 [54] to describe the exchange-correlation effect. It follows that $a = 3.282$ Å and $c = 5.301$ Å for the lattice parameters of wurtzite ZnO and 129.97 GPa for the bulk modulus, which are in good consistency with the theoretical values and experimental results [55].

The influence of oxygen partial pressure on the surface kinetics is accounted for by taking two reconstructed ZnO(0001) surfaces as the substrates of the homoepitaxial growth. The surfaces are described by slab models consisting of five stoichiometric Zn-O double layers plus one topmost incomplete layer. The topmost layer of the (2 × 2)-O reconstruction, as shown in Fig. 1(a), is characteristic of an oxygen atom adsorbed at one of the hollow sites in each (2 × 2) surface cell, hereafter referred as reconstructed oxygen (O_r). In contrast, the topmost layer of the n_3 surface consists of an equilaterally triangular pit in each (4 × 4) surface cell, three oxygen ions at the edge of each side of the pit as shown in Fig. 1(b). Although the size of the triangles may be different in reality, the main kinetic features are expected to be the same for this type of reconstruction containing triangular holes.

To minimize the interaction between neighboring adatoms, a (4 × 4) supercell is used for both reconstructed surfaces. The (2 × 2)-O and n_3 surfaces thus have stoichiometry of $Zn_{80}O_{84}$ and $Zn_{90}O_{93}$, respectively, in our slab models. A Γ-centered 3 × 3 k-point mesh is used to sample the surface Brillouin zone. To avoid the spurious charge transfer, pseudo-H atoms with a valence of $\frac{1}{2}e^-$ are introduced to saturate the O-terminated side of the slab $(000\bar{1})$. A vacuum layer of 20 Å is included to avoid the interaction of slabs in the normal direction. The atoms in the bottom two double layers and the pseudo H atoms are fixed, while the other atoms are allowed to relax until the forces are less than 0.02 eV/Å. The diffusion properties are calculated by the nudged elastic band method (NEB) [56].

To compare the relative stability of surface morphology with different stoichiometric ratio, we define the formation free energy of the surface system as $\Delta G = E_{\text{tot}} - T_s S - \sum_i N_i \mu_i$, where E_{tot} is the total energy of the surface system, T_s the temperature of the surface, S the entropy of the surface atoms, and N_i is the number of surface atoms of species i with corresponding chemical potential μ_i. Assuming Zn and O atoms are in thermal equilibrium with ZnO bulk, μ_{Zn} and μ_{O} are mutually dependent as $\mu_{\text{Zn}} + \mu_{\text{O}} = E_{\text{ZnO}}$. By choosing oxygen molecule as a reference of the chemical potential of oxygen, $\mu_{\text{O}} = \frac{1}{2}E_{\text{O}_2} + \Delta\mu_{\text{O}}$, it follows that

$$\Delta G = E_{\text{tot}} - T_s S - N_{\text{Zn}} E_{\text{ZnO}} + (N_{\text{Zn}} - N_{\text{O}})(\tfrac{1}{2}E_{\text{O}_2} + \Delta\mu_{\text{O}}). \quad (1)$$

The upper and lower bounds of $\Delta\mu_{\text{O}}$ are limited by the formation of O_2 molecules and Zn bulk metal, respectively, i.e., $E_{\text{ZnO}} - E_{\text{Zn}} - \frac{1}{2}E_{\text{O}_2} \leqslant \Delta\mu_{\text{O}} \leqslant 0$, where E_{ZnO}, E_{Zn}, and E_{O_2} are the total energy of ZnO bulk, Zn bulk, and oxygen molecule, respectively. According to our DFT calculations, we obtain -3.05 eV $\leqslant \Delta\mu_{\text{O}} \leqslant 0$. Experimentally, $\Delta\mu_{\text{O}}$ is determined by P_{O_2} and T, i.e., the oxygen partial pressure

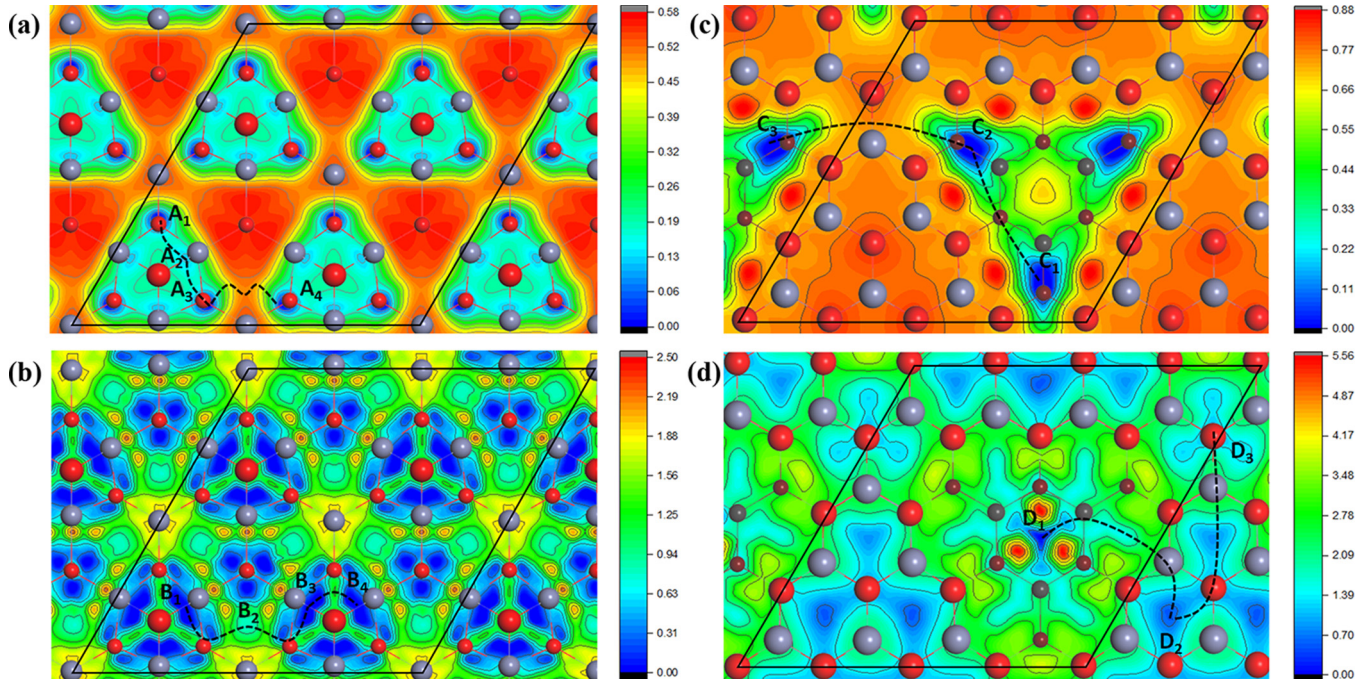

FIG. 2. Contour plots of the potential energy surface (PES) of an adatom on ZnO(0001) surfaces. (a) Zn adatom on (2×2)-O; (b) O adatom on (2×2)-O; (c) Zn adatom on n_3; (d) O adatom on n_3. The long dashed curves schematically show the diffusion pathways used in the NEB calculations, along which the labels $A/B/C/D_i$ mark the local minimum sites. The denotations of the parallelogram boxes and the spheres are the same in Fig. 1.

and the temperature of the gas phase, respectively. Following the same approach in previous papers [57–59] and referring the NIST website [60] and CODATA table [61], the chemical potential of oxygen at temperature T can be correlated with the oxygen partial potential logarithmically.

III. RESULTS

The potential energy surfaces (PES) of the Zn and O adatom are constructed according to the total energy of the surface with the adatom at the uniform grid sites, by optimizing the surface and the normal coordinate of the adatom. According to the contour plots of the PES as shown in Fig. 2, a common feature of the two surfaces is that the O adatom has more (meta)stable adsorption sites than the Zn adatom does. Moreover, the variation of the adsorption energy of O adatom is more pronounced compared to that of Zn adatom. However, the (meta)stable adsorption sites are different for the two surfaces. On the (2×2)-O surface, the Zn adatom resides around the reconstructed oxygen O_r, whereas the O adatom prefers to be around either O_r or the substrate oxygen atom far away from O_r. On the n_3 surface, the stable adsorption sites of Zn atom are at the corner of the triangular pit, while O adatom prefers the geometric center of the lower layer and is metastable on the upper layer.

To obtain the most stable structures with the adatom, full relaxation has been carried out from the sites of the lowest total energies, marked as A_1–D_1 in Fig. 2. It turns out that A_1 is not the most stable adsorption site for Zn on (2×2)-O. The Zn adatom pushes O_r away from the hexagonal center and forms a Zn-O_r dimer with a bond length of 1.89 Å. Meanwhile, one of the three bonds between O_r and the surface Zn atoms is broken, as can be seen in Fig. 3(a). The O adatom on (2×2)-O also tends to bind with O_r and form an O-O_r dimer as shown in Fig. 3(b), with a bond length of 1.47 Å. On the n_3 surface, the most stable Zn adatom forms two Zn-O bonds with the surface O at the corner of the triangular pit, as shown in Fig. 3(c). The bond lengths are about 2.06 Å. In contrast, the O adatom on the n_3 surface binds with the substrate much weaker, with apparent bond lengths of about 2.39 Å. As a result of the weak interaction, the neighboring Zn or O atoms on the substrate relax toward or away from the O adatom, respectively, as can be seen in Fig. 3(d). However, the relaxation of n_3 surface induced by Zn or O adatom is smaller than that of the (2×2)-O surface. As a result, the most stable adsorption sites of Zn and O on n_3 are still close to the minima sites C_1 and D_1, respectively.

The adsorption energy of Zn or O adatom on the reconstructed surfaces is defined as the change of the formation free energy of the surface system upon surface adsorption. According to Eq. (1), the adsorption energy of Zn and O on the surface is expressed as

$$\Delta G_a^{\mathrm{Zn}} = \left(E_{\mathrm{tot}}^a - E_{\mathrm{tot}}^s - E_{\mathrm{ZnO}} + \tfrac{1}{2}E_{\mathrm{O}_2}\right) + \Delta\mu_{\mathrm{O}},$$
$$\Delta G_a^{\mathrm{O}} = \left(E_{\mathrm{tot}}^a - E_{\mathrm{tot}}^s - \tfrac{1}{2}E_{\mathrm{O}_2}\right) - \Delta\mu_{\mathrm{O}}, \qquad (2)$$

where E_{tot}^a and E_{tot}^s are the total energies of the reconstructed surfaces after and before the adatom adsorption, respectively. Meanwhile, the relative stability of the two reconstructions also depends on the chemical potential of oxygen. According to Eq. (1), the difference of the formation free energy of the two surfaces is expressed as

$$\Delta\Gamma = \Delta G_{(2\times2)\text{-O}} - \Delta G_{n_3} = \Delta E - T_s\Delta S - \Delta\mu_{\mathrm{O}}, \qquad (3)$$

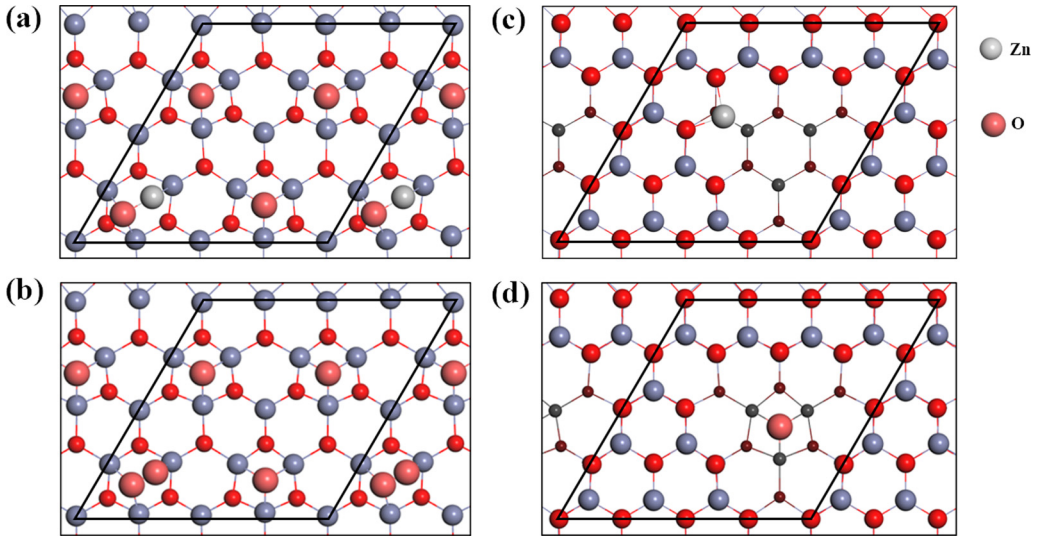

FIG. 3. Surface structure after adatom adsorption on the ZnO(0001) surface. (a) Zn adatom on (2×2)-O; (b) O adatom on (2×2)-O; (c) Zn adatom on n_3; (d) O adatom on n_3. The denotations of the parallelogram boxes and the spheres are the same in Fig. 1.

where $\Delta E = E_{\text{tot}}^{(2\times2)\text{-O}} - E_{\text{tot}}^{n_3} + 10E_{\text{ZnO}} - \frac{1}{2}E_{\text{O}_2}$. As a starting point, we temporarily ignore the influence of entropy and obtain $\Delta\mu_{\text{O}}^{\text{cri}} = -0.71$ eV. When $\Delta\mu_{\text{O}}$ is smaller than $\Delta\mu_{\text{O}}^{\text{cri}}$, the system tends to form n_3 structure; otherwise, the system prefers (2×2)-O reconstruction. Therefore, it is reasonable to use the two reconstructed surfaces to sample the oxygen-rich condition and the oxygen-poor conditions.

The lowest adsorption energies of Zn and O on the two surfaces as functions of $\Delta\mu_{\text{O}}$ are plotted in Fig. 4. The corresponding values of oxygen partial pressure at 500, 800, and 1000 K are shown on the upper x axis to connect the chemical potential with the real experimental condition. The vertical dotted line corresponds to $\Delta\mu_{\text{O}}^{\text{cri}}$. It can be observed that in the (2×2)-O preferred region, adsorption of O is always more favorable than adsorption of Zn, although it is exothermic only at the oxygen-rich limit. In the n_3 preferred region, however, the adsorption of Zn and O atom is exothermic in the oxygen-poor condition and in the oxygen-rich region on the left of the dotted lines, respectively. As stable adsorption is a prerequisite for maintaining the surface growth, it suggests that the growth of ZnO occurs more easily at the two extremes of oxygen-poor and oxygen-rich conditions and in a small middle window, and different growth mechanism proceeds under different oxygen partial pressure. The entropy contribution at finite temperature favors the (2×2)-O reconstruction, as a consequence of the higher vibrational entropy of surface adatoms in the adatom structure as reported before [45]. Therefore, a smaller $\Delta\mu_{\text{O}}^{\text{cri}}$ is expected and the dotted line in Fig. 4 would move leftward with increasing temperature. It means that the middle window for stable oxygen adsorption on n_3 shrinks at a higher temperature.

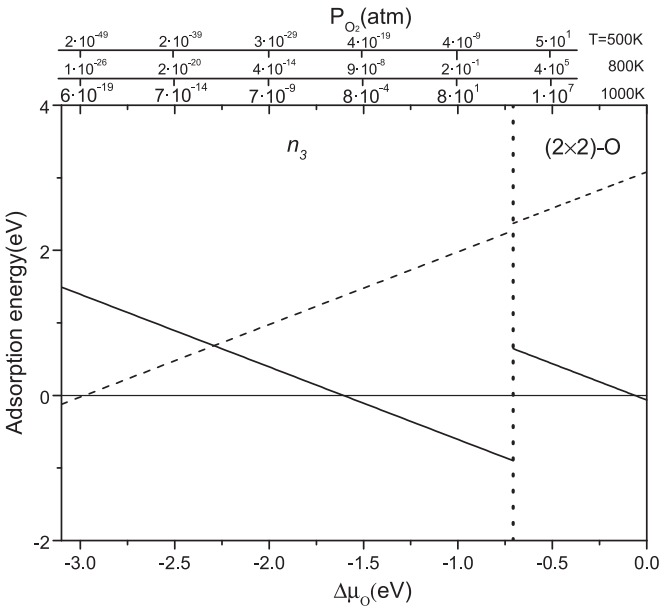

FIG. 4. The adsorption energies of Zn (dashed lines) and O (solid lines) as functions of the chemical potential of oxygen. The vertical dotted line marks $\Delta\mu_{\text{O}}^{\text{cri}} = -0.71$ eV when the formation free energy of the (2×2)-O and that of the n_3 are equal. The corresponding values of oxygen partial pressure at 500, 800, and 1000 K are shown on the upper side of x axis.

Besides the surface adsorption, sufficient surface diffusion is necessary for growth of a smooth surface. The pathways accounting for the main characteristics of the surface diffusion are identified according to the PES, as marked by the dashed curves and the symbols in Fig. 2. The convergent energy barriers of these diffusion pathways are calculated by NEB method and shown in Fig. 5. On the (2×2)-O surface, it is obvious that diffusion barriers are highest when the adatoms move from the site around one O_r to that around another O_r, with diffusion barriers of 0.56 and 1.58 eV for Zn and O atoms, respectively. On n_3 surface, in contrast, the bottleneck of the surface diffusion occurs when the adatoms hop across the O-terminated step edge of the triangular pits. The maximal diffusion barriers of Zn and O between neighboring minima on n_3 are 0.69 and 3.78 eV, respectively.

The diffusion properties of Zn and O adatoms on Zn(0001) surface are summarized in Table I. Two conclusions can be

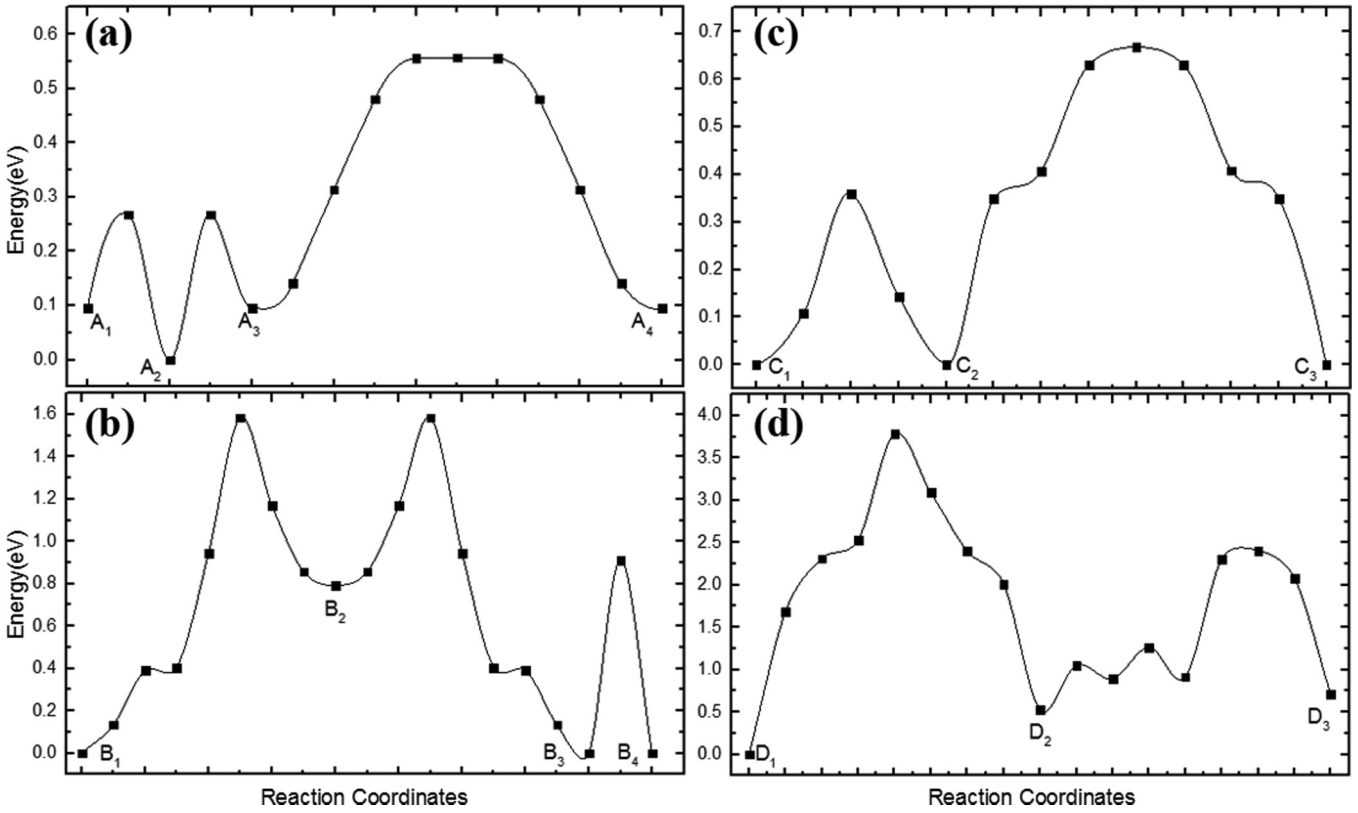

FIG. 5. Energetic profiles of an adatom diffusing on ZnO(0001) surface. (a) Zn adatom on (2×2)-O; (b) O adatom on (2×2)-O; (c) Zn adatom on n_3; (d) O adatom on n_3. The diffusion pathways and symbols are marked in Fig. 2. Note that A_2 becomes more stable than $A_{1(3)}$ after full relaxation.

reached. First, the diffusion energy barrier of Zn is always smaller than that of O adatom, no matter what the oxygen partial pressure is. It suggests that the deposition of O atoms determines the nucleation rate, while the diffusion of Zn atoms determines the growth processes. Previous studies have predicted that Zn is more diffusion than O [46,62] in bulk ZnO and within the oxygen-terminated ZnO(0001) surface [48]. Together with our results, it is possible to conclude that the Zn is always more mobile than O both in bulk ZnO and on the surfaces. Second, the diffusion of the adatom on (2×2)-O is easier than on n_3, either for Zn atom or for O atom. Since the specific surface reconstructions depend on the oxygen partial pressure, it indicates that the diffusion coefficients of both Zn and O adatom increase with the partial pressure of oxygen. The results are not only consistent with our experiments [26], but also consistent with the chemical potential dependence of the Zn diffusivity in bulk ZnO [47].

Generally speaking, insufficient surface diffusion keeps the surface far from equilibrium and leads to a high nucleation rate [51]. It has been well established that sufficient surface diffusion is necessary for smooth growth morphology, whereas lower surface diffusivity leads to rougher morphology and smaller characteristic size of as-grown microstructures [33,50]. Therefore, our results suggest that in comparison with the oxygen-rich scenario, growth in oxygen-poor condition is more likely to follow the three-dimensional island mode and thus result in a rougher surface. Indeed, the previous experiments have reported that oxygen-rich condition is required to obtain smooth surface on ZnO(0001), which are in consistent with our results [23–26]. Since the physical properties of the surface microstructure are affected by the morphology, understanding the influence of the oxygen partial pressure on the growth mechanism would help us to obtain the desirable properties of metal oxides.

TABLE I. The diffusion energy barriers of Zn and O adatoms on the two reconstructed ZnO(0001) surfaces, in units of eV.

Condition	Reconstruction	Zn	O
Oxygen-rich	(2×2)-O	0.56	1.58
Oxygen-poor	n_3	0.69	3.78

IV. SUMMARY

In summary, two typical surface reconstructions of Zn-terminated ZnO(0001) surface are utilized to model the influence of the oxygen partial pressure on surface kinetics of ZnO. By calculating the potential energy surfaces of Zn or O adatom on the two surfaces, we find that the adsorption of O atom is favorable compared to that of Zn adatom when reconstruction (2×2)-O is preferred under the oxygen-rich condition. In contrast, the relative stability of Zn and O adatom depends on the oxygen partial pressure when n_3 is preferred under the oxygen-poor condition. Combining with NEB

calculations, we conclude that Zn adatom is more diffusive than O on both surfaces. Besides, both Zn and O adatom diffuse more rapidly on (2×2)-O than on n_3 surface. It indicates that the diffusion coefficients of Zn or O atom decrease with decreasing partial pressure of oxygen, which would result in a rougher surface. We expect that the results are enlightening to understand the influence of partial pressure of oxygen in fabrication of microstructures of zinc oxide and other metal oxides.

ACKNOWLEDGMENTS

The numerical calculations have been carried out at the High Performance Computing Center of Nanjing University and National Supercomputing Center in Tianjin. This work was supported by the NSF of China (Grants No. 11174123, No. 11474157, No. 11674155, and No. 11634005), the Basic Research Project of Jiangsu Province (Grant No. BK20161390), and the Ministry of Science and Technology of China (Grant No. 2017YFA0303702).

[1] X. Yu, T. J. Marks, and A. Facchetti, Nature Mater. **15**, 383 (2016).
[2] M. Willander, O. Nur, Q. X. Zhao, L. L. Yang, M. Lorenz, B. Q. Cao, J. Z. Pérez, C. Czekalla, G. Zimmermann, M. Grundmann *et al.*, Nanotechnology **20**, 332001 (2009).
[3] S. C. Rai, K. Wang, Y. Ding, J. K. Marmon, M. Bhatt, Y. Zhang, W. Zhou, and Z. L. Wang, ACS Nano **9**, 6419 (2015).
[4] T. Gao and T. H. Wang, Appl. Phys. A **80**, 1451 (2005).
[5] G. Shen, P.-C. Chen, K. Ryu, and C. Zhou, J. Mater. Chem. **19**, 828 (2009).
[6] E. Comini, Anal. Chim. Acta **568**, 28 (2006).
[7] E. Palomares, J. N. Clifford, S. A. Haque, T. Lutz, and J. R. Durrant, J. Am. Chem. Soc. **125**, 475 (2003).
[8] T. Tsuji and M. Hirohashi, Appl. Surf. Sci. **157**, 47 (2000).
[9] P. Zeman and S. Takabayashi, Surf. Coat. Tech. **153**, 93 (2002).
[10] D. G. Syarif, A. Miyashita, T. Yamaki, T. Sumita, Y. Choi, and H. Itoh, Appl. Surf. Sci. **193**, 287 (2002).
[11] Y. Ma, G. T. Du, T. P. Yang, D. L. Qiu, X. Zhang, H. J. Yang, Y. T. Zhang, B. J. Zhao, X. T. Yang, and D. L. Liu, J. Cryst. Growth **255**, 303 (2003).
[12] R. J. Hong, H. J. Qi, J. B. Huang, G. B. He, Z. X. Fan, and J. A. Shao, Thin Solid Films **473**, 58 (2005).
[13] S. Kim, W. I. Lee, E.-H. Lee, S. K. Hwang, and C. Lee, J. Mater. Sci. **42**, 4845 (2007).
[14] Y. M. Tao, S. Y. Ma, H. X. Chen, J. X. Meng, L. L. Hou, Y. F. Jia, and X. R. Shang, Vacuum **85**, 744 (2011).
[15] S. K. Pandey, S. K. Pandey, U. P. Deshpande, V. Awasthi, A. Kumar, M. Gupta, and S. Mukherjee, Semicond. Sci. Technol. **28**, 085014 (2013).
[16] Y. A. K. Reddy, A. S. Reddy, and P. S. Reddy, J. Alloy Comp. **583**, 396 (2014).
[17] H. Lu, P. Zhou, H. Liu, L. Zhang, Y. Yu, Y. Li, and Z. Wang, Mater. Lett. **165**, 123 (2016).
[18] H. Liu, P. Zhou, L. Zhang, Z. Liang, H. Zhao, and Z. Wang, Mater. Lett. **164**, 509 (2016).
[19] S. A. Chambers, Adv. Mater **22**, 219 (2010).
[20] A. Ohtomo and H. Y. Hwang, Nature **427**, 423 (2004).
[21] H. Y. Dang, J. Wang, and S. S. Fan, Nanotechnology **14**, 738 (2003).
[22] S. Mraz and J. M. Schneider, J. Appl. Phys. **100**, 023503 (2006).
[23] H. Kato, M. Sano, K. Miyamoto, and T. Yao, Jpn. J. Appl. Phys. **42**, L1002 (2003).
[24] H. Xu, K. Ohtani, M. Yamao, and H. Ohno, Appl. Phys. Lett. **89**, 071918 (2006).
[25] H.-J. Ko, T. Yao, Y. Chen, and S.-K. Hong, J. Appl. Phys. **92**, 4354 (2002).
[26] D. Shu, X. Xiang, M. Liu, and M. Wang, Phys. Rev. B **96**, 115411 (2017).
[27] Z. L. Wang, J. Phys-Condens. Mat. **16**, R829 (2004).
[28] Z. L. Wang, Mater. Today **7**, 26 (2004).
[29] P. Yang, H. Yan, S. Mao, R. Russo, J. Johnson, R. Saykally, N. Morris, J. Pham, R. He, and H.-J. Choi, Adv. Funct. Mater. **12**, 323 (2002).
[30] X. Liu, X. Wu, H. Cao, and R. P. H. Chang, J. Appl. Phys. **95**, 3141 (2004).
[31] M. Liu, C. Meng, Z.-H. Xue, X. Xiong, D.-J. Shu, R.-W. Peng, Q. Wu, Z. Hu, and M. Wang, Europhys. Lett. **104**, 18004 (2013).
[32] M. Liu, G.-B. Ma, X. Xiong, Z.-W. Wang, R.-W. Peng, J.-G. Zheng, D.-J. Shu, Z. Zhang, and M. Wang, Phys. Rev. B **87**, 085306 (2013).
[33] D.-J. Shu, X. Xiong, Z.-W. Wang, Z. Zhang, M. Wang, and N.-B. Ming, J. Phys. Chem. C **115**, 31 (2011).
[34] Z. Wang, N. Pan, Z. Li, and J. Yang, J. Chem. Phys. **139**, 124704 (2013).
[35] C. Noguera, J. Phys-Condens. Matt. **12**, R367 (2000).
[36] J. Goniakowski, F. Finocchi, and C. Noguera, Rep. Prog. Phys. **71**, 016501 (2008).
[37] H. Xu, L. Dong, X. Q. Shi, M. A. Van Hove, W. K. Ho, N. Lin, H. S. Wu, and S. Y. Tong, Phys. Rev. B **89**, 235403 (2014).
[38] H. Zheng, M. Gruyters, E. Pehlke, and R. Berndt, Phys. Rev. Lett. **111**, 086101 (2013).
[39] R. Wahl, J. V. Lauritsen, F. Besenbacher, and G. Kresse, Phys. Rev. B **87**, 085313 (2013).
[40] H. Meskine and P. A. Mulheran, Phys. Rev. B **84**, 165430 (2011).
[41] J. H. Lai, S. H. Su, H.-H. Chen, J. C. A. Huang, and C.-L. Wu, Phys. Rev. B **82**, 155406 (2010).
[42] M.-H. Du, S. B. Zhang, J. E. Northrup, and S. C. Erwin, Phys. Rev. B **78**, 155424 (2008).
[43] O. Dulub, U. Diebold, and G. Kresse, Phys. Rev. Lett. **90**, 016102 (2003).
[44] G. Kresse, O. Dulub, and U. Diebold, Phys. Rev. B **68**, 245409 (2003).
[45] M. Valtiner, M. Todorova, G. Grundmeier, and J. Neugebauer, Phys. Rev. Lett. **103**, 065502 (2009).
[46] P. Erhart and K. Albe, Appl. Phys. Lett. **88**, 201918 (2006).
[47] A. Azarov, V. Venkatachalapathy, Z. Mei, L. Liu, X. Du, A. Galeckas, E. Monakhov, B. G. Svensson, and A. Kuznetsov, Phys. Rev. B **94**, 195208 (2016).
[48] G.-Y. Huang, C.-Y. Wang, and J.-T. Wang, Chin. Phys. B **19**, 013101 (2010).

[49] K. Fujiwara, A. Ishii, T. Abe, and K. Ando, J. Appl. Phys. **112**, 064301 (2012).
[50] J. Tersoff, A. W. Denier van der Gon, and R. M. Tromp, Phys. Rev. Lett. **72**, 266 (1994).
[51] I. V. Markov, *Crystal Growth for Beginners* (World Scientific, Singapore, 2003), 2nd ed.
[52] G. Kresse and J. Furthmüller, Comp. Mater. Sci. **6**, 15 (1996).
[53] G. Kresse and J. Furthmüller, Phys. Rev. B **54**, 11169 (1996).
[54] J. P. Perdew, J. A. Chevary, S. H. Vosko, K. A. Jackson, M. R. Pederson, D. J. Singh, and C. Fiolhais, Phys. Rev. B **46**, 6671 (1992).
[55] Ü. Özgür, Y. I. Alivov, C. Liu, A. Teke, M. A. Reshchikov, S. Doğan, V. Avrutin, S.-J. Cho, and H. Morkoc, J. Appl. Phys. **98**, 041301 (2005).
[56] G. Mills, H. Jónsson, and G. K. Schenter, Surf. Sci. **324**, 305 (1995).
[57] K. Reuter and M. Scheffler, Phys. Rev. B **65**, 035406 (2001).
[58] Z. F. Hou, D. J. Shu, G. L. Chai, T. Ikeda, and K. Terakura, J. Phys. Chem. C **118**, 19795 (2014).
[59] G. L. Chai, Z. Hou, D. J. Shu, T. Ikeda, and K. Terakura, J. Am. Chem. Soc. **136**, 13629 (2014).
[60] M. W. J. Chase, NIST-JANAF Thermochemical Tables, 4th, Vol. 9 (1998).
[61] J. D. Cox, D. D. Wagman, and V. A. Medvedev, *CODATA Key Values for Thermodynamics* (Hemisphere Publishing Corporation, Washington, DC, 1989).
[62] P. Erhart and K. Albe, Phys. Rev. B **73**, 115207 (2006).